http://dx.doi.org/10.5012/bkcs.2012.33.1.143

Photodissociation of C_3H_5Br and C_4H_7Br at 234 nm

Hyun Kook Kim, Dababrata Paul, Kiryong Hong, Hana Cho, Kyoung-Seok Lee,† and Tae Kyu Kim*

Department of Chemistry and Center for Functional Materials, Pusan National University, Busan 609-735, Korea
**E-mail: tkkim@pusan.ac.kr*
†Division of Metrology for Quality Life, Korea Research Institute of Standards and Science, Daejeon 305-340, Korea
Received November 5, 2011, Accepted November 12, 2011

The photodissociation dynamics of cyclopropyl bromide (C_3H_5Br) and cyclobutyl bromide (C_4H_7Br) at 234 nm was investigated. A two-dimensional photofragment ion-imaging technique coupled with a [2+1] resonance-enhanced multiphoton ionization scheme was utilized to obtain speed and angular distributions of the nascent $Br(^2P_{3/2})$ and $Br^*(^2P_{1/2})$ atoms. The recoil anisotropies for the Br and Br^* channels were measured to be $\beta_{Br} = 0.92 \pm 0.03$ and $\beta_{Br^*} = 1.52 \pm 0.04$ for C_3H_5Br and $\beta_{Br} = 1.10 \pm 0.03$ and $\beta_{Br^*} = 1.49 \pm 0.05$ for C_4H_7Br. The relative quantum yield for Br was found to be $\Phi_{Br} = 0.13 \pm 0.03$ and for C_3H_5Br and C_4H_7Br, respectively. The soft radical limit of the impulsive model adequately modeled the related energy partitioning. The nonadiabatic transition probability from the 3*A*' and 4*A*' potential energy surfaces was estimated and discussed.

Key Words : Photodissociation, Cycloalkyl Halides, Curve-crossing, C_s symmetry, Ion-imaging

Introduction

Photodissociation dynamics of organic halides in the ultraviolet (UV) region has prompted extensive experimental and theoretical investigations aiming at elucidating the mechanism of formation of halogen atoms in the ground and excited spin-orbit coupling states.[1-10] As a prototype for depicting numerous types of photodissociations in a variety of polyatomic molecules, the photodissociation of methyl halide (CX_3Y; X = H, D, F:Y = Br, I) in the A-band has been intensively studied.[11-13] Its A-band owing to the $\sigma^* \leftarrow n$ transition is composed of three optically accessible states: $^1Q_1(3E)$, $^3Q_0(2A_1)$, and $^3Q_1(2E)$ in descending order of energy.[14] They are repulsive in nature, leading to the prompt/impulsive dissociation of the C–Y bond. In the adiabatic limit, the $^3Q_0(2A_1)$ state correlates with the spin-orbit excited $Y^*(^2P_{1/2})$ channel in which the related transition dipole moment is aligned parallel to the C–Y bond axis, and others with the $Y(^2P_{3/2})$ channel where the corresponding transitions are polarized perpendicular to the C–Y bond. Curve crossing occurs between $^1Q_1(3E)$ and $^3Q_0(2A_1)$ surfaces which arises from the symmetry reduction of the parent molecule during dissociation. As the symmetry is lowered from the intrinsic C_{3v} to C_s, the $^1Q_1(3E)$ state splits into two components, 4*A*' and 2*A*". The $^3Q_1(2E)$ state splits into 2*A*' and 1*A*". The $^3Q_0(2A_1)$ state is reduced to 3*A*'. It has been proposed that the symmetry lowering motion such as *e*-type bending vibration induces the symmetry to be reduced and a fraction of molecules consequently dissociates *via* the surfaces in C_s symmetry.[4,5,10,15,16]

Cycloalkyl halides are mono-halogenated cyclic ring molecules which has intrinsic C_s symmetry. In particular, the photodissociation dynamics of cyclopropyl iodide was investigated at 266 and 280 nm using ion-imaging of nascent iodine atoms.[17] In another study, state-selective photofragment translational spectroscopy of cyclohexyl iodide was performed and the energy difference between the equatorial and axial conformers was determined by monitoring I and I^* fragments at several excitation wavelengths.[18] Recently photodissociation dynamics of cyclopentyl bromide has been studied by velocity ion imaging method.[19] However, detailed dissociation dynamics of mono-halogenated cycloalkanes has not yet been elucidated and more information is necessary to explain and to gain a detailed understanding of the photodissociation dynamics of cycloalkyl halides in A-band. Due to the intrinsic C_s symmetry of cycloalkyl halides, the nonadiabatic dissociation dynamics should be explained in terms of interaction between involved potential energy surfaces in C_s symmetry.[10,15]

In this work, we investigate the photodissociation dynamics of cyclopropyl bromide (C_3H_5Br) and cyclobutyl bromide (C_4H_7Br) at 234 nm. The nascent Br and Br* atoms were selectively detected using a [2+1] resonance-enhanced multiphoton ionization (REMPI) scheme. The relative quantum yield for the Br and Br^* channels were measured. Their speed and angular distributions were obtained by use of a velocity map ion-imaging technique. The results provide an insight into the photodissociation dynamics of cycloalkyl halides with C_s symmetry, and can be applied to the photodissociation of other complicated multihalogenated cycloalkanes.

Experiment

The experimental setup has been described in detail elsewhere.[9,10] Our velocity mapping apparatus consists of a supersonic molecular beam source, time-of-flight (TOF) spectrometer, and a position sensitive detector. A C_3H_5Br or C_4H_7Br (Aldrich, 99%) molecular beam with a pulse width of 180 μs was obtained using 1% of the gas mixture seeded

in He buffer and was operated at 10 Hz. The experiment was performed using one-color scheme. Linearly polarized UV laser light was produced by doubling of the Nd:YAG laser (Spectra Physics, GCR-170) pumped dye laser (Lumonics HD 500) output using a BBO crystal and was aligned utilizing a half-wave retardation plate. The UV laser light with a typical energy of 50-100 μJ/pulse was focused perpendicularly onto the molecular beam in the ionization region by lens with a 150 mm focal length. A single UV laser pulse excited C_3H_5Br or C_4H_7Br molecules and ionized resultant Br and Br^* fragments. The [2+1] REMPI technique employed to selectively ionize Br (233.7 nm, *via* $6p\ ^4P_{3/2}$ intermediate state) and Br^* (234.0 nm, *via* the intermediate state of $6p\ ^4D_{1/2}$).[20]

Resultant Br fragment were accelerated using a repeller, an extractor, and a ground electrode. The nonhomogeneous electric field around electrodes functioned as an electrostatic ion lens[21] to create an image on a two-dimensional position-sensitive detector that was composed of a dual chevron microchannel plate (MCP), a phosphor screen (Galileo Electrooptic Corp. 3040FM), an image intensifier, and a charge-coupled device (CCD) camera. A synchronously triggering pulse was applied to the image intensifier in order to segregate Br ion signals from background noises caused by scattering light and ions with different masses. More than 10^4 shots were averaged to construct an image. TOF mass spectra were collected using a photomultiplier tube and a digital oscilloscope instead of the image intensifier and the CCD camera. To minimize background noises, images and

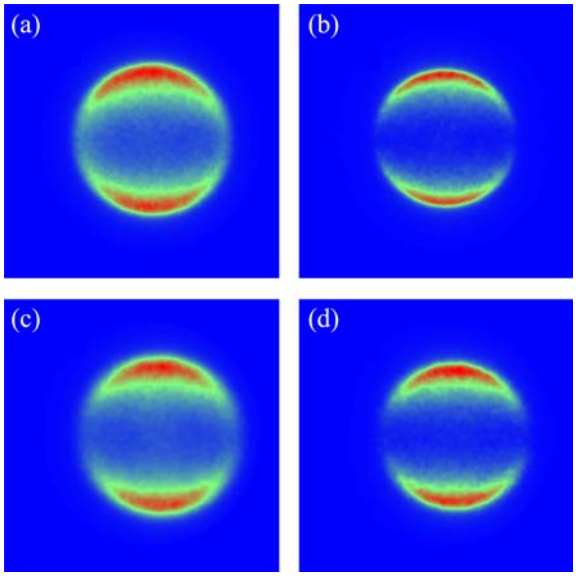

Figure 1. Raw ion images of (a) Br and (b) Br^* from the photodissociation of C_3H_5Br. Those of Br and Br^* from C_4H_7Br are shown in (c) and (d), respectively. In all images, the polarization vector of the photolysis laser is vertical.

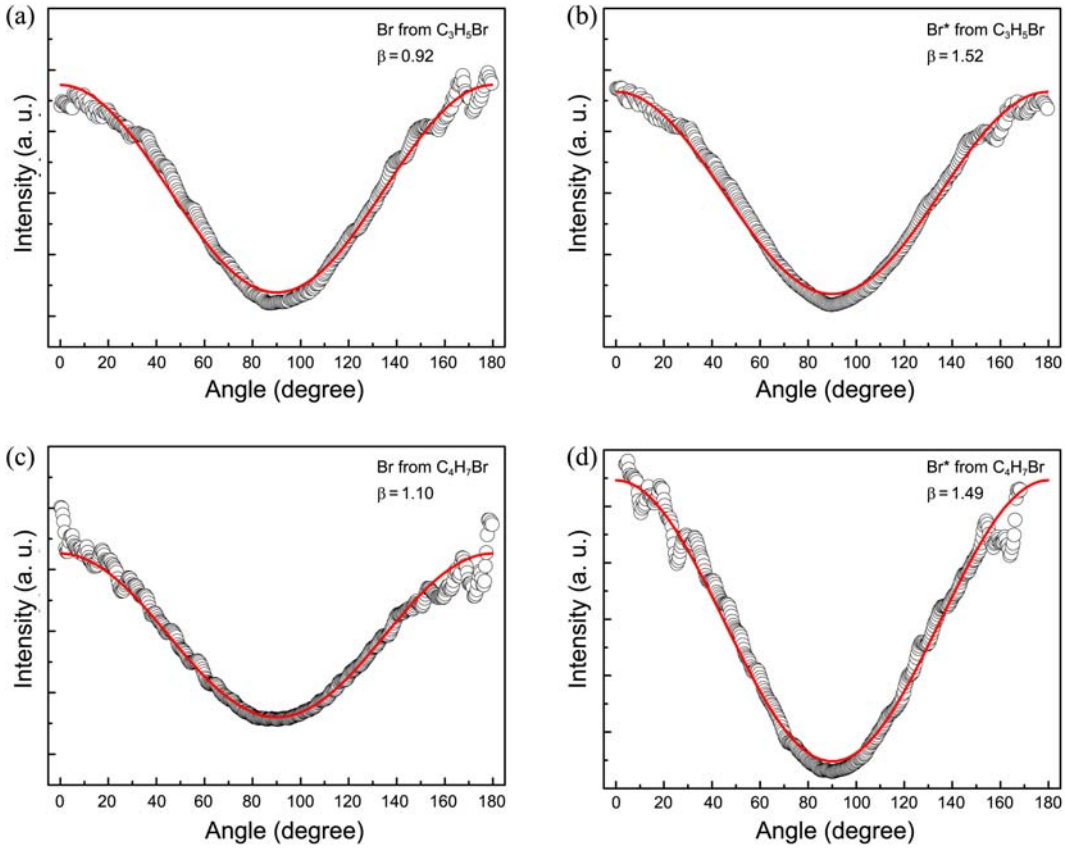

Figure 2. Angular distributions for (a) Br and (b) Br^* channels in the photodissociation of C_3H_5Br at 234 nm. Those of Br and Br^* from C_4H_7Br are shown in (c) and (d), respectively. The open circles are the experimental data and the anisotropy parameters are extracted by the fitting curves (red solid lines).

spectra contained at off-resonance wavelengths under the same condition were subtracted from those at resonance wavelengths. All images and spectra were averaged over a range of 2 cm^{-1} to cover all velocity components of Br atoms.

Results

Raw Images and Recoil Anisotropies. The raw images of Br and Br^* obtained from the photolysis of C_3H_5Br/C_4H_7Br at 234 nm are presented in Figure 1. Since the polarization of the photolysis laser beam was aligned vertically, distinct polar-cap appearances in all images indicate that Br/Br^* from C_3H_5Br/C_4H_7Br photolysis were produced almost *via* parallel transition. In order to extract the recoil anisotropy, the raw ion image has been processed using an inverse Abel transformation. The intensity of the components with velocity at proper ranges has been integrated at individual angles. The resultant angular distributions are plotted in Figure 2. The recoil anisotropy, β, has been extracted by fitting the angular distribution with the formula,[22]

$$P(\theta) = 1 + \beta P_2(\cos\theta), \quad (1)$$

where $P(\theta)$ is the integrated intensity at the angle θ and is a second-order Legendre polynomial. β varies from 2 for the limit of a parallel transition and to −1 for that of a perpendicular transition. As shown in Figure 2, the anisotropy parameters determined for the overall ranges of velocity distributions are $\beta_{Br} = 0.92 \pm 0.03$ and $\beta_{Br^*} = 1.52 \pm 0.04$ for C_3H_5Br. For C_4H_7Br, $\beta_{Br} = 1.10 \pm 0.03$ and $\beta_{Br^*} = 1.49 \pm 0.05$ are obtained.

Translational Energy Distributions. The total translational energy distribution based on a center-of-mass coordinate, $P(E)$, is obtained by converting the speed distribution, $P(v)$, according to the equations:

$$P(E) = P(v) = \frac{dv}{dE} \propto \frac{P(v)}{v} \quad (2)$$

$$E_T = \frac{1}{2}(m_{Br} + m_R)\left(\frac{m_{Br}}{m_R}\right)v_{Br}^2 . \quad (3)$$

where R denotes C_3H_5 for C_3H_5Br and C_4H_7 for C_4H_7Br. $P(v)$ is extracted by integrating the reconstructed 3D speed distribution over all angles at each speed. The total translational energy distributions for Br and Br^* from C_3H_5Br and C_4H_7Br are plotted in Figure 3. Each distribution in Figure 3 was well fitted by a *single* Gaussian distribution, indicating that the bromine fragments are produced *via* direct dissociation on the repulsive surfaces. The average translation energy, $\langle E_T \rangle$, for the Br and Br^* from C_3H_5Br is determined to be 76.85 and 65.51 kJ/mol, respectively. For C_4H_7Br, $\langle E_T \rangle_{Br}$ = 67.10 kJ/mol and $\langle E_T \rangle_{Br}$ = 58.86 kJ/mol are obtained. To calculate the fraction of the translational energy of Br to the available energy (f_T), the following relationship was used:

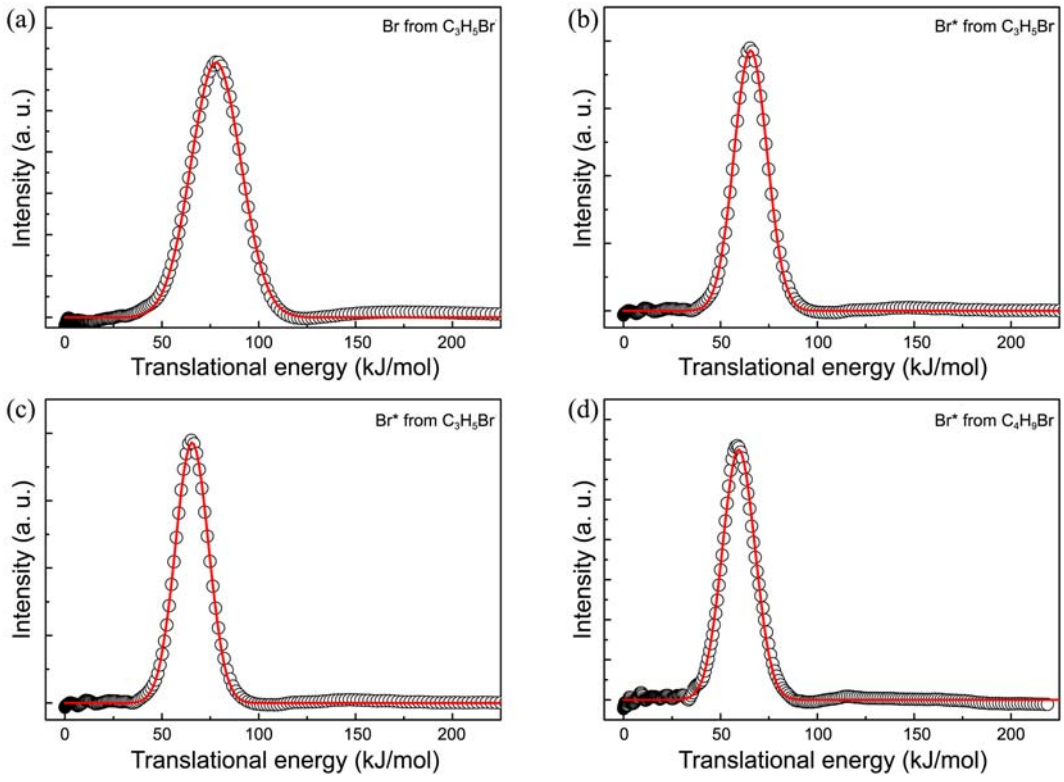

Figure 3. Total translational energy distributions for (a) Br and (b) Br^* in the photodissociation of C_3H_5Br at 234 nm. Those of Br and Br^* from C_4H_7Br are shown in (c) and (d), respectively. Each data point (open circle) corresponds to the relative intensity by integrating values for all angular components at a specific translational energy. The red solid lines indicate the curves fitted with a Gaussian-shaped function.

Table 1. Average translational energies, energy fractions, recoil anisotropy parameters, and relative quantum yields of Br and Br* resulting from the photolysis of C_3H_5Br and C_4H_7Br at 234 nm. The energy unit is kJ/mol. f_T is the fraction of the translational energy to the available energy measured in this work. Numbers in parentheses are the errors corresponding to one standard deviation

Channel	E_{avl}	$\langle E_T \rangle$	f_T	β	Φ
C_3H_5 + Br	209.00	76.85	0.37	0.92(0.03)	–
C_3H_5 + Br*	165.50	65.51	0.40	1.52(0.04)	0.13(0.03)
C_4H_7 + Br	237.21	67.10	0.29	1.10(0.03)	–
C_4H_7 + Br*	193.03	58.86	0.30	1.49(0.05)	0.18(0.02)

$$f_T = \frac{\langle E_T \rangle}{E_{avl}} \tag{4}$$

$$E_{avl} = h\nu - D_0 - E_{el} + E_{int} \tag{5}$$

where E_{avl} and $h\nu$ designates the available energy of the photodissociation and the photon energy of 234 nm, respectively. The parameter D_0 indicates the dissociation energy of the C–Br bond; a value of D_0 = 72.9 kJ/mol and 69.3 kJ/mol based on the density functional theory (DFT) at B3LYP/6-311++G(d,p) level,[23,24] was chosen for C_3H_5Br and C_4H_7Br, respectively. The electronic energy, E_{el}, is equal to the appropriate electronic energy level of atomic bromine, and was chosen to be 0 for Br and 44.1 kJ/mol for Br*. Because rotational and vibrational excitations are negligible in a supersonic molecular beam, the internal energy, E_{int}, was set to zero. The average translation energies and f_T values of Br/Br* channels for C_3H_5Br and C_4H_7Br are listed in Table 1.

Relative Quantum Yields. The relative quantum yields are defined as follows:

$$\Phi_{Br} = \frac{N_{Br}}{N_{Br} + N_{Br^*}}, \tag{6}$$

$$\Phi_{Br^*} = 1 - \Phi_{Br}, \tag{7}$$

where N_X is the number of species X (X = Br, Br*). These numbers were extracted from the relative [2+1] REMPI ion signal intensities of Br and Br* in the TOF spectra, yielding values of $\Phi_{Br} = 0.13 \pm 0.03$ for C_3H_5Br and 0.18 ± 0.02 for C_4H_7Br. The extracted relative quantum yields are also listed in Table 1.

Discussion

As shown in Figure 3, the total energy distributions for Br and Br* from photolysis of C_3H_5Br and C_4H_7Br are well characterized by single-peaked Gaussian functions. The f_T values from C_3H_5Br were 0.37 for Br and 0.40 for Br*. From C_4H_7Br, f_T = 0.29 and 0.30 were obtained for Br and Br* formation channels, respectively. These f_T values indicate that a considerable portion of the available energy is partitioned into the internal degrees of freedom of the R (R = C_3H_5 or C_4H_7) fragments. Based on these findings, the 234 nm dissociation dynamics of C_3H_5Br seems to be similar to that of C_4H_7Br. The energy partitioning in the dissociation *via* repulsive potential can be explained by invoking two

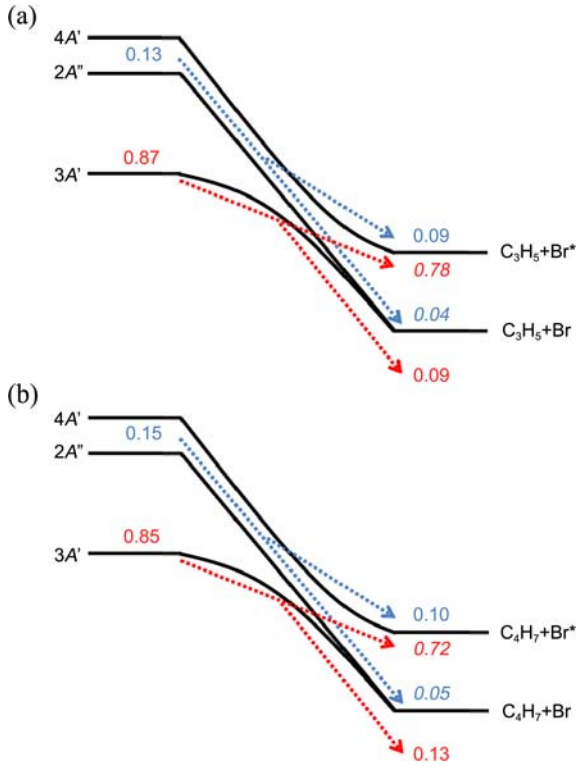

Figure 4. Schematic diagram of the photolyses of (a) C_3H_5Br and (b) C_4H_7Br on the 3*A*' and [4*A*', 2*A*"] electronic states. Dotted lines show the trajectories along individual pathways. The numbers represent the fraction of molecules for different dissociation pathways.

radical limits of the impulsive model. The rigid radical limit ignore the energy flow onto the vibration energy of the fragments, and thereby the upper limit of f_T. If we apply the rigid radical limit to the photodissociation of C_3H_5Br and C_4H_7Br, the fraction of the energy into the translational energy (f_T^{rigid}) is calculated by the following relationship:[25-27]

$$f_T^{rigid} = \left(1 + \frac{I_R}{\mu_R r_{c.m.}^2 \sin^2\chi}\right)^{-1}, \tag{8}$$

$$f_T^{rigid} = 1 - f_{int}^{rigid}, \tag{9}$$

where I_R is the moment of inertia of the R(C_3H_5 or C_4H_7) fragment about an axis through its center-of-mass (c.m.) and perpendicular to the plane defined by the c.m., Br atom, and the a-carbon atom where the bromine atom is attached. The parameter $\mu_{R\text{-}Br}$ is the reduced mass of the R and bromine fragments, and $r_{c.m.}$ is the distance from the c.m. of the R fragment to the α-carbon atom. Using geometrical parameters optimized by density functional theory (DFT) at B3LYP/6-311++G(d,p) level,[24] we estimate values of f_{int}^{rigid} = 0.13(f_T^{rigid} = 0.87) for C_3H_5Br and f_{int}^{rigid} = 0.01(f_T^{rigid} = 0.99) for C_4H_7Br at the rigid radical limit. As shown in Table 1, these values are very different from the findings for the Br/Br* formations from C_3H_5Br and C_4H_7Br. This fact indicates that the dissociation process involves considerable vibrational excitation of the photofragments. Therefore, the

soft radical limit,[26,27] which considers the vibrational excitation of fragments, could be applied to the C_3H_5Br and C_4H_7Br. Using the soft radical limit, values of $f_T^{soft} = \mu_{C\text{-}Br}/\mu_{C_3H_5\text{-}Br} = 0.38$ for C_3H_5Br and $f_T^{soft} = \mu_{C\text{-}Br}/\mu_{C_4H_7\text{-}Br} = 0.32$ for C_4H_7Br were determined, where $\mu_{A\text{-}B}$ is the reduced mass of the A and B fragments. The soft radical limit of the impulsive model seems more appropriate for predicting energy partitioning in the photodissociations of C_3H_5Br and C_4H_7Br at 234 nm. Although there is no a priori reason for the agreement between the values predicted using the soft radical limit and those measured in this work, this fact strongly suggests that vibrational excitation should be considered in the photodissociations of C_3H_5Br and C_4H_7Br, which is related with the shape of the related potential energy surfaces involved in the nonadiabatic transition.[28]

Since the total energy distributions for Br and Br* from photolysis of C_3H_5Br and C_4H_7Br are well characterized by single-peaked Gaussian functions, it is therefore reasonable to assume that at 234 nm the $\sigma^* \leftarrow n$ type of electronic transition localized on the C–Br chromophore is excited here as in the simplest alkyl bromides.[5,10,13] The recoil anisotropy parameters observed in this study ($\beta_{Br} = 0.92 \pm 0.03$ and $\beta_{Br^*} = 1.52 \pm 0.04$ from C_3H_5Br and $\beta_{Br} = 1.10 \pm 0.03$ and $\beta_{Br^*} = 1.49 \pm 0.05$ from C_4H_7Br) are less than the limiting value of parallel transition ($\beta_{lim}^{\parallel} = +2$), indicating that both perpendicular and parallel transitions are responsible for generation of Br and Br* from C_3H_5Br and C_4H_7Br. The relative contributions of the parallel and perpendicular transitions to the obtained anisotropy parameters can be calculated from the following relationship:

$$\begin{pmatrix} \beta_{Br} \\ \beta_{Br^*} \end{pmatrix} = \begin{pmatrix} C_{Br}^{\parallel} & C_{Br}^{\perp} \\ C_{Br^*}^{\parallel} & C_{Br^*}^{\perp} \end{pmatrix} \begin{pmatrix} \beta_{lim}^{\parallel} \\ \beta_{lim}^{\perp} \end{pmatrix} \quad (10)$$

where $C_N^M (M = \perp, \parallel; N = Br, Br^*; C_N^{\perp} + C_N^{\parallel} = 1)$ is the relative fraction of the species N generated by either the parallel ($\parallel$) or perpendicular ($\perp$) transition. $\beta_{lim}^{\parallel}$ and $\beta_{lim}^{\perp}$ are the limit values of the anisotropy parameters for the parallel and perpendicular transitions, respectively. As mentioned before, the electronic transition of C_3H_5Br and C_4H_7Br at 234 nm is a $\sigma^* \leftarrow n$ transition mainly localized on the C–Br bond. Therefore, a limiting value for the parallel transition can be deduced from that of the Br* generated in the 234 nm photodissociation of CF_3Br.[15] It has been known that only $^3Q_0$ (pure parallel component) is responsible for the generation of Br* in the photodissociation of CF_3Br at 234 nm. As a result, $\beta_{lim}^{\parallel} = 1.8$ was chosen for the analysis. On the same account, $\beta_{lim}^{\perp} = -1/2\,\beta_{lim}^{\parallel} = -0.9$ was selected. The use of limiting values is not rigorous for repulsive dissociation of polyatomic molecule, especially when a significant fraction of energy appears in internal energy of fragment.[27] Nevertheless, this approach helps one to interpret the data qualitatively and discuss the related dynamic processes during photodissociation. As results, from C_3H_5Br, 67% (33%) of Br evolves from the parallel (perpendicular) transition and 90% (10%) of Br* arise from the initial parallel (perpendicular) transition. For the C_4H_7Br case, 74% (26%) of Br evolves from the parallel (perpendicular) transition and 88% (12%) of Br* arise from the initial parallel (perpendicular) transition. To investigate the origins of the transitions, the excited states pertinent to the absorption at 234 nm must be conjectured. The excited states of C_3H_5Br and C_4H_7Br at 234 nm can be inferred from the simplest organic halides, remembering that the C–Br moiety acts as the main chromophore at 234 nm.

There are three optically accessible states of CH_3Br are denoted $^1Q_1$, $^3Q_0$, and $^3Q_1$, in descending order of energy.[13,29] As discussed, in molecules with intrinsic C_s symmetry, the $^3Q_1$ state splits into the 2A' and 1A" states. The $^3Q_0$ state does not split and is directly correlated with the 3A' state. The $^1Q_1$ state is correlated with the 4A' and 2A" states in the C_s symmetry. In the UV spectrum of CH_2BrCl,[5,30] the absorption band of lowest [2A', 1A"] ($^3Q_1$) states is shifted to significant longer wavelengths compared to the $^3Q_1$ state of CH_3Br. Another feature is that the 3A' ($^3Q_0$) and [4A' and 2A"] ($^1Q_1$) states are very close and have nearly equal widths for CH_2BrCl. Since C_3H_5Br and C_4H_7Br are also of intrinsic C_s symmetry, the potential energy surfaces reached *via* the transition localized on the C–Br bond seem to be similar to those in CH_2BrCl. As with CH_2BrCl, the 3A' ($^3Q_0$) and [4A' and 2A"] ($^1Q_1$) states of C_3H_5Br and C_4H_7Br are accessible at 234 nm excitation.[5] The 4A' and 2A" states are responsible for the electronic transitions aligned perpendicular to the C–Br bond and correlate with the channel for Br formation, whereas the $3A' \leftarrow 1A'$ transition is polarized parallel to the bond and correlates with the Br* channel.[5] However, in C_s symmetry, an avoided crossing can be formed between the 3A' and 4A' surfaces. As a consequence, 234 nm excitation leads to Br production *via* three pathways (3A', 2A", and a nonadiabatic transition from 4A' to 3A'), and to Br* production *via* two pathways (4A' and a nonadiabatic transition from 3A' to 4A'). The nonadiabatic transition from the 3A' to 4A' results in the generation of the parallel component for the Br* channel. In addition, the nonadiabatic transition from the 4A' to 3A' results in the generation of the perpendicular observed for the Br channel.

The fractions of the dissociation pathways leading to the generation of the parallel and perpendicular components of Br and Br* have been extracted using following relationship:

$$\begin{pmatrix} \Phi_{Br}C_{Br}^{\parallel} & \Phi_{Br}C_{Br}^{\perp} \\ \Phi_{Br^*}C_{Br^*}^{\parallel} & \Phi_{Br^*}C_{Br^*}^{\perp} \end{pmatrix} = \begin{pmatrix} f_{3A'\leftarrow 3A'} & f_{3A'\leftarrow 4A'} + f_{2A''\leftarrow 2A''} \\ f_{4A'\leftarrow 3A'} & f_{4A'\leftarrow 4A'} \end{pmatrix} \quad (11)$$

where $f_{A\leftarrow B}$ (A, $B = 3A'$, $4A'$, $2A''$) is the fraction of molecules that dissociate *via* the A and B surfaces before and after the crossing point, respectively, and $\Sigma_{A,B} f_{A\leftarrow B} = 1$. Then the curve-crossing probability were calculated using,

$$P_{up} = \frac{f_{4A'\leftarrow 3A'}}{f_{4A'\leftarrow 3A'} + f_{3A'\leftarrow 3A'}}$$

$$P_{down} = \frac{f_{3A'\leftarrow 4A'}}{f_{4A'\leftarrow 4A'} + f_{3A'\leftarrow 4A'}} \leq \frac{f_{3A'\leftarrow 4A'} + f_{2A''\leftarrow 2A''}}{f_{4A'\leftarrow 4A'} + f_{3A'\leftarrow 4A'} + f_{2A''\leftarrow 2A''}} \quad (12)$$

Table 2. Fractions of molecules dissociating *via* individual pathways and curve-crossing probabilities in the photodissociations of C_3H_5Br and C_4H_7Br at 234 nm

Molecule	$f_{3A'\leftarrow 3A'}$	$f_{3A'\leftarrow 4A'}+f_{2A''\leftarrow 2A''}$	$f_{4A'\leftarrow 4A'}$	$f_{4A'\leftarrow 3A'}$	P_{up}	P_{down}
C_3H_5Br	0.09	0.04	0.09	0.78	0.90	≤ 0.31
C_4H_7Br	0.13	0.05	0.10	0.72	0.85	≤ 0.33

where P_{up} and P_{down} are probability of nonadiabatic transitions from the lower to the upper and from the upper and the lower surfaces, respectively. The resultant fractions and curve crossing probabilities from photolyses of C_3H_5Br and C_4H_7Br are listed in Table 2. $P_{up} = 0.90$ and $P_{down} \leq 0.31$ (hence 0.31 is the upper limit of P_{down}) for C_3H_5Br and $P_{up} = 0.85$ and $P_{down} \leq 0.33$ for C_4H_7Br may be indicative of the difference between the up and down crossing probabilities, which is contrary to the Landau-Zener model.[31] Similar results have been observed for the dissociations of CH_3Br and CH_3I, in which the difference between the up and down crossing probabilities was attributed to the symmetry reduction from C_{3v} to C_s caused by zero-point motion along *e*-symmetry modes or the excitation of vibrational bending modes.[4,15,28,32] This finding indicates that there are significant vibrational excitations of fragments which are in agreements with observed f_T values. To unravel the relationship[33] between the vibrational excitation of the products and the shape of the related potential energy surfaces involved in the photodissociation of C_3H_5Br and C_4H_7Br, further theoretical investigation is in progress.

Summary

The photodissociations of C_3H_5Br and C_4H_7Br have been investigated at 234 nm using a photofragment ion-imaging technique coupled with a REMPI scheme. The nascent Br and Br^* atoms were detected after C–Br dissociation *via* the $\sigma^* \leftarrow n$ transition localized on the C–Br bond. The total translational energy distributions for Br and Br^* pathways from C_3H_5Br and C_4H_7Br were found to be well modeled by single Gaussian distribution. The energy partitioning in this process was well modeled by the soft radical limit of the impulsive model, suggesting that a significant amount of energy is partitioned into the vibrational degrees of freedom of the fragments. Based on the recoil anisotropy parameters and relative quantum yields, the relative contributions of the parallel and perpendicular transitions to the generation of bromine fragments have been extracted for the Br and Br^* pathways from C_3H_5Br and C_4H_7Br. Using these values, the fractions of the dissociation pathways leading to the generation of the parallel and perpendicular components of Br and Br^* have been calculated. The nonadiabatic transition probability from the 3*A*' and 4*A*' potential energy surfaces was estimated to be 0.90 and 0.85 for C_3H_5Br and C_4H_7Br, respectively.

Acknowledgments. This work was supported by the Korea Research Foundation Grant (KRF-2008-314-C00161).

References

1. Molina, M. J.; Rowland, F. S. *Nature* **1974**, *248*, 810.
2. Garcia, R. R.; Solomon, S. *J. Geophys. Res.* **1994**, *99*, 12937.
3. Tzeng, W. B.; Lee, Y. R.; Lin, S. M. *Chem. Phys. Lett.* **1994**, *227*, 467.
4. Kim, T. K.; Lee, K. W.; Lee, K. S.; Lee, E. K.; Jung, K. H. *Chem. Phys. Lett.* **2007**, *446*, 31.
5. Zou, P.; McGiven, W. S.; North, S. W. *Phys. Chem. Chem. Phys.* **2000**, *2*, 3785.
6. Blanchet, V.; Samartzis, P. S.; Wodtke, A. M. *J. Chem. Phys.* **2009**, *130*, 034304.
7. Hua, L.; Shen, H.; Zhang, C.; Cao, Z.; Zhang, B. *Chem. Phys. Lett.* **2008**, *460*, 50.
8. Lee, K. S.; Lee, K. W.; Lee, S. K.; Jung, K. H.; Kim, T. K. *J. Mol. Spectra.* **2008**, *249*, 43.
9. Paul, D.; Kim, H. K.; Hong, K.; Kim, T. K. *Bull. Korean Chem. Soc.* **2011**, *32*, 659.
10. Lee, S. K.; Paul, D.; Hong, K.; Cho, H. N.; Jung, K. W.; Kim, T. K. *Bull. Korean Chem. Soc.* **2009**, *30*, 2962.
11. Eppink, A. T. J. B.; Parker, D. H. *J. Chem. Phys.* **1999**, *110*, 832.
12. Eppink, A. T. J. B.; Parker, D. H. *J. Chem. Phys.* **1998**, *109*, 4758.
13. Gougousi, T.; Samartzis, P. C.; Kitsopoulos, T. N. *J. Chem. Phys.* **1998**, *108*, 5742.
14. Mulliken, R. S. *J. Chem. Phys.* **1940**, *8*, 382.
15. Kim, T. K.; Park, M. S.; Lee, K. W.; Jung, K. H. *J. Chem. Phys.* **2001**, *115*, 10745.
16. Lee, K. W.; Jee, Y. J.; Jung, K. H. *J. Chem. Phys.* **2002**, *115*, 4490.
17. Arnold, P. A.; Cosofret, B. R.; Dylewski, S. M.; Houston, P. L.; Carpenter, B. K. *J. Phys. Chem. A* **2001**, *105*, 1693.
18. Freitas, J. E.; Hwang, H. J.; Ticknor, A. B.; Elsayed, M. A. *Chem. Phys. Lett.* **1991**, *183*, 165.
19. Ghazal, A. Y.; Liu, Y.; Wang, Y.; Hu, C.; Zhang, B. *Chem. Phys. Lett.* **2011**, *511*, 39.
20. Park, M. S.; Jung, Y. J.; Lee, S. H.; Kim, D. C.; Jung, K. H. *Chem. Phys. Lett.* **2000**, *322*, 429.
21. Eppink, A. T. J. B.; Parker, D. H. *Rev. Sci. Instrum.* **1997**, *68*, 3477.
22. Zare, R. N.; Herschbach, D. R. *Proc. IEEE* **1963**, *51*, 173.
23. Becke, A. D. *Phys. Rev. A* **1988**, *38*, 3098.
24. Lee, C.; Yang, W.; Parr, R. G. *Phys. Rev. B* **1988**, *37*, 785.
25. Busch, G. E.; Wilson, K. R. *J. Chem. Phys.* **1972**, *56*, 3626.
26. Busch, G. E.; Wilson, K. R. *J. Chem. Phys.* **1972**, *56*, 3638.
27. Busch, G. E.; Wilson, K. R. *J. Chem. Phys.* **1972**, *56*, 3655.
28. Amatatsu, Y.; Yabushita, S.; Morokuma, K. *J. Chem. Phys.* **1996**, *104*, 9783.
29. Mulliken, R. S. *J. Chem. Phys.* **1935**, *3*, 513.
30. McGiven, W. S.; Li, R.; Zou, P.; North, S. W. *J. Chem. Phys.* **1999**, *111*, 5771.
31. Landau, L. D.; Lifshitz, E. M. *Quantum Mechanics 3*; Pergamon: New York, 1997.
32. Felder, P. *Chem. Phys. Lett.* **1992**, *197*, 425.
33. Amatatsu, Y.; Morokuma, K. *J. Chem. Phys.* **1991**, *94*, 4858.